RSC Advances

ROYAL SOCIETY OF CHEMISTRY

www.rsc.org/advances

Journal Name

RSCPublishing

ARTICLE

Improved Chemical Stability of Silver by Selective Distribution of Silver Particles on Reduced Graphene Oxide Nanosheets†

Cite this: DOI: 10.1039/xoxxoooooox

Received ooth January 2012,
Accepted ooth January 2012

DOI: 10.1039/xoxxoooooox

www.rsc.org/

Xiu-Zhi Tang,[a] Xuelong Chen,[b] Gang Wu,[a] Xiao Hu[b]* and Jinglei Yang[a]*

The chemical stability of particles on reduced graphene oxide (RGO) nanosheets is an important issue for the RGO/particles hybrid materials. Here we report that the chemical stability of environmentally sensitive silver can be significantly improved by control the distribution of silver particles on RGO nanosheets. By switching the sequence of "deoxygenation" and "deposition", two kinds of RGO/silver hybrids are prepared. The structure and chemical state of silver particles on RGO are investigated by X-ray diffraction, X-ray photoelectron spectroscopy, thermogravimetric analysis, Ultraviolet-Visible spectroscopy, Raman spectra and Scanning Electron Microscope. It is found that the graphene/Ag hybrid prepared by "deposition" and then "deoxygenation" can still exhibit obvious surface enhanced Raman scattering (SERS) signals after 10-month storage, comparing with the hybrid material that fabricated in inverse order. The selective distribution of silver particles and non-uniform dispersion of electrons on RGO nanosheets are responsible for the different performances. This study provides a new insight into preparing chemically stable RGO/particle hybrid materials.

Introduction

Due to its high conductivity, large specific surface area, excellent chemical stability and mechanical flexibility, graphene has been widely used as an ideal substrate for particle loading.[1, 2] In the last few years, graphene/particles hybrid materials were exploited and exhibited synthetic effect on their optical, catalytic and conductive performances.[3-9] The chemical stability of the attached particles on graphene nanosheets is a fundamental and important issue for their functional applications. Silver as an excellent noble metal possesses many amazing properties and a number of researchers focus their attentions on developing reduced graphene oxide (RGO)/silver hybrids with various applications.[10-13] However, the chemical instability of silver is a serious obstacle for the performances of RGO/silver hybrid materials. As we known, the oxidation of silver can increase interface contact resistance, weaken plasmon resonances and damage the optical property.[14, 15]

Fortunately, the protective effects of graphene have been exploited and demonstrated to be effective to suppress silver from being oxidized.[14-19] Thermal oxidation stability and chemical stability of silver nanowires (AgNW)-RGO transparent electrode can be significantly improved due to the gas-barrier of RGO according to the report of Liu et al.[15] Actually, researchers found the size of RGO nanosheets can affect the protection of silver. Zhang et al confirm that larger size of RGO sheets show better oxidation resistance than those RGO sheets with smaller size and the hybrid materials can preserve a low sheet resistance of 27 $\Omega \cdot sq^{-1}$ after annealing at 700 ^{o}C.[17] Moreover, as it can tune localized surface plasmon resonance from visible to NIR, silver is one of the most promising materials for plasmon devices, especially for surface-enhanced Raman scattering (SERS)[14, 20, 21] However, the oxidation of silver can dampen its plasmonic characters seriously. In many recent cases, single layer (or few layers) of graphene grown by chemical vapor deposition (CVD) is proved to be a stable layer for preventing silver from oxidation and the SERS property of silver/graphene hybrid can be preserved.[14, 17, 18, 22] With the aid of monolayer graphene, the surface-enhanced Raman scattering (SERS) signals of Rhodamine B (RhB) on silver can be largely stabilized for up to 28 days.[17] So far, although the oxidation barrier role of graphene synthesized by CVD method have been investigated and exhibits excellent protecting effect for silver, few researchers note the diversity of chemical stability between those silver particles attached on RGO nanosheets. According to Zahed et al's report, the silver particles can be stabilized on thiolated RGO as the strong interaction between thiol groups and particles.[23] Similarly, polyethylenimine-modified RGO were proved to be an ideal substrate for anchoring silver particles with stable antibacterial effects.[24] Nevertheless, the interaction between residual oxygen moieties on RGO nanosheets and attached nanoparticles has been discussed in our previous works.[25, 26] These oxygen-containing groups are confirmed to have an obvious effect on the size, distribution, quantity and crystalline structure of decorated silver particles. Especially, the oxygen moieties have an obviously binding effect on the formation of metal particles from their liquid precursors, leading the particles preferentially locate around the oxygen-containing groups.[25-28] Based on these

observations, the strategy that switching the sequence of "deoxygenation" and "deposition", which are two basic reactions for the preparation of RGO/particles hybrid materials, is adapted to make particles selectively deposit on RGO nanosheets and extra functionalization of RGO is unnecessary.

In this paper, we demonstrate the chemical stability of particles from RGO/silver hybrid materials prepared with inverse sequence of "deoxygenation" and "deposition" are obviously different. To make operation of switching more convenient, DMF was chosen since it has been demonstrated to be a good solvent for GO or RGO, effective reductant for silver ions, and also possess high boiling point that is critical for the solvothermal reduction of GO nanosheets.[29, 30] We confirm the chemical stability of silver particle can be greatly improved by choosing suitable sequence of "deoxygenation" and "deposition". With the correct sequence, SERS signals of RGO/silver can be maintained for at least 10 months.

Experimental

2.1 Materials

Sulfuric acid (A.R 95-98%), potassium permanganate (A.R.), silver nitrate (A.R.) ethanol (A.R.) and N,N-dimethylformamide (A.R.) were purchased from Sigma-Aldrich (Singapore). Natural graphite flakes with an average diameter of 48 μm were supplied by Huadong Graphite Factory (China). Rhodamine B (RhB), sodium nitrate (99%) was provided by Alfa Aesar Company. Hydrogen peroxide (30%) was supplied by VMR Company. All chemicals were used as received.

2.2 Preparation of graphene oxide

Graphene oxide (GO) was prepared using the modified hummer method according the previous reports.[31, 32] Firstly, natural graphite powders (2.5 g) with sodium nitrate (2.5 g) were mixed by 120 ml concentrated H_2SO_4 in an ice bath. Then, $KMnO_4$ (15 g) was divided into five equal parts and added slowly into above slurry with continuous stirring. After that, the mixture was allowed to react at 35 ^oC for 6 hours and then 150 ml deionized water was added carefully to avoid boiling. The diluted solution was maintained around 95 ^oC for 15 min and then the suspension was poured into a beaker with 700 ml DI water inside. For purification, H_2O_2 (60 ml, 30 %) was added into solution, then the obtained yellow solution was washed by diluted hydrochloric (10 wt%), dialysed for one week and centrifuged with DI water until pH of supernatant is close to 7. The obtained graphene oxide was dried at 80 ^oC before grinded into powders.

2.3 Synthesis of reduced graphene oxide/silver hybrids

Graphene oxide powers were added into 100 ml DMF and then treated in a probe sonicator for 30 minutes to form a stable suspension with a concentration of 0.5 mg/ml. The mixture of GO and DMF was firstly treated at 153 ^oC and refluxed for 1 hour to obtain the RGO. After the temperature decrease to about 60 ^oC, 50 ml $AgNO_3$ solution (188 mM) was added and refluxed with vigorous stirring. Then, the suspension was filtrated by a Teflon membrane (bore diameter = 0.2 μm) and washed by water and ethanol repeatedly. The final product was obtained by drying the solid powder in a vacuum oven at 60 ^oC overnight. The sample fabricated by the above method was termed as GAD-AR. Another hybrid material, named as GAD-RA, was prepared by the same procedures except that the order of "deoxygenation" and "deposition" was swapped. Briefly, the GO solution was first mixed with $AgNO_3$ and the reaction was operated at 60 ^oC for 1 hour. To avoid the interference from the unreacted silver ions, the mid-product of GAD-AR was filtrated and washed by DMF. Afterwards, the same volume of fresh DMF was added and then the temperature was raised to 153 ^oC and refluxed for 1 hour. The product GAD-RA was obtained after filtration, washing and drying. Considering the fact that the hybrid materials are usually dispersed in ethanol to prepare SERS samples, part of the GAD-RA or GAD-AR was thus kept separately in ethanol for 10 months and then filtrated, washed by ethanol and dried at 60 ^oC in a vacuum oven overnight. The final materials via 10-month storage were named as GAD-RA-10 m and GAD-AR-10 m according to their storage period.

2.4 Characterizations

The morphologies of GAD-AR, GAD-RA, GAD-AR-10 m and GAD-RA-10 m were observed using JOEL JSM-7600F Scanning Electron Microscope (SEM). X-ray diffraction (XRD) patterns were measured by a Bruker D8 Advanced XRD using Cu Kα1 radiation. High resolution X-ray photoelectron spectroscopy (XPS) with monochromatic Al Kaas as X-ray excitation source operating at 15 kV and 10 mA was used to characterize the surface compositions of GAD-AR, GAD-RA, GAD-AR-10 m and GAD-RA-10 m. Ultraviolet visible (UV-Vis) spectra of GAD aqueous solution was measured by a SP752-PC UV–VIS spectrophotometer over the wavelength range from 200 to 800 nm. Raman spectra were measured using a Renishaw inVia Raman microscope by the excitation wavelength of 514.5 nm. The samples for SERS measurement were prepared as follows: GAD-AR, GAD-RA, GAD-AR-10 m and GAD-RA-10 m were soaked in an ethanol solution of RhB with a concentration of 1×10^{-5} M for 1 h and the resultant samples were dried, washed by deionized water and then measured by the Raman microscope.

Results and discussion

3.1 Synthesis of RGO/silver hybrid materials

The strategy for the synthesis of GAD-AR and GAD-RA with different order of "deoxygenation" and "reduction" are illustrated in Fig. 1. For GAD-AR, silver particles were firstly deposited on the GO nanosheets and then the substrate was reduced. By contrast, for the GAD-RA, GO was reduced at first and silver particles were subsequently attached onto RGO. Due to the nonuniform dispersion of residual oxygen-containing groups on RGO nanosheets and their constrained effect on the decorated particles, RGO/silver hybrids prepared with different sequences of "deoxygenation" and "deposition" can make silver particles selectively deposit on different region of RGO nanosheets. The silver particles from GAD-AR are supposed to be mainly located on the rich oxygen-containing groups region while those particles from GAD-RA should be randomly distributed on the DMF reduced graphene oxide sheets.

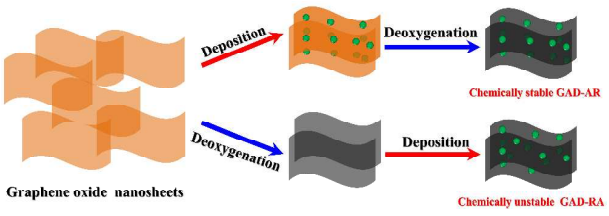

Fig. 1. Schematic processes to prepare GAD-AR and GAD-RA.

UV-Vis spectrum was utilized to demonstrate DMF is an effective reductant for both graphene and silver ions. Two characteristic peaks located at ~230 and ~300 nm, caused by π to π* transitions of the C=C and n to π* transitions of the C=O can be observed separately from the UV-Vis curves of GO (Fig. 2a).[33] As the evidence of GO being reduced, the corresponding peaks reflected on the GAD-RA and the GAD-AR shifted to ~270 nm, implying the recovery of the electron conjugation within the GO nanosheets. Moreover, the peaks centred at 413 and 428 nm corresponding to the surface plasmon resonance of silver particles on the GAD-AR and GAD-RA, respectively. It's noted that these two peaks are not geometrically symmetric, indicating that the silver particles on RGO nanosheets possess a wide size distribution.[34] Observed from the TEM images shown in Fig. 2b-e, the average diameter of silver particles is 67 nm for GAD-RA and 74 nm for GAD-RA, which is consistent with the results of UV-Vis.

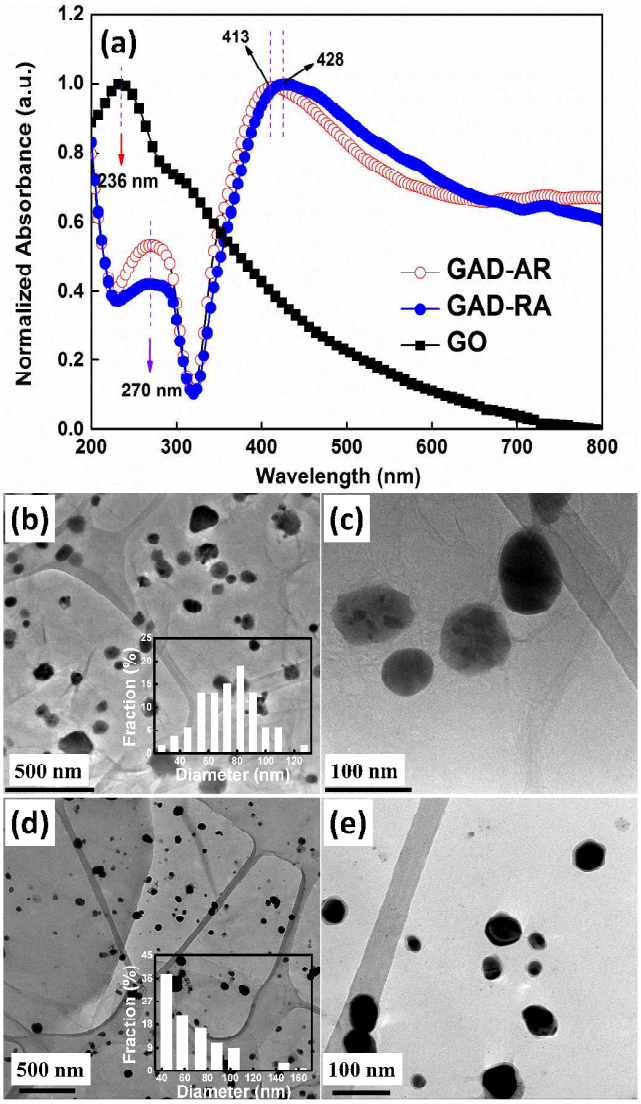

Fig. 2. (a) UV-Vis spectra of GO, GAD-AR and GAD-RA. TEM images of GAD-RA (b-c) and GAD-AR (d-e). The insets shown in (b) and (d) are histogram of particles size distribution.

3.2 Characterizations and chemical stability of RGO/silver hybrid materials

It was reported that silver particles attached onto the RGO surface can act as the "hot-spot" and make the hybrid materials an ideal candidate for the SERS performances.[35] In present work, SERS signals of RGO/silver hybrids were collected, and the RhB was chosen as the analyte. As shown in Fig. 3a, the typical peaks at 1279, 1357, 1562 and 1645 cm^{-1}, attributed to the RhB, are apparently observed for both GAD-AR and GAD-RA, indicating excellent SERS activity of hybrid materials. Interestingly, we found the SERS effect changed when we collect the Raman signals from those hybrid materials preserved for 10 months. From Fig. 3b, the signals of RhB can still be distinguished from the Raman spectrum of GAD-AR-10 m, but few peaks ascribed to RhB can be seen on Raman curve of GAD-RA-10 m. According to previous reports, it's widely accepted that the oxidation of silver is a serious barrier for the SERS activity as it can decrease surface plasmon resonance intensity.[14, 17] Thus, we conclude that the silver particles on GAD-AR possess much better chemical stability than those on GAD-RA. To confirm this, further characterizations were performed to check whether the attached silver on hybrid materials has been oxidized.

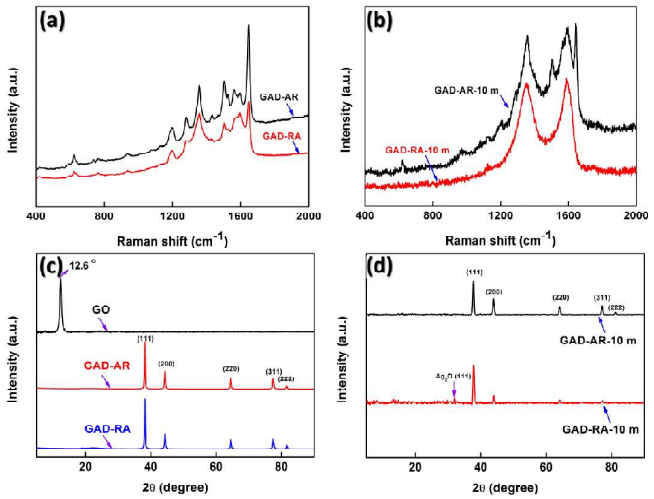

Fig. 3. SERS spectra of (a) GAD-AR and GAD-RA, (b) GAD-AR-10 m and GAD-RA-10 m; XRD patterns of (c) GO, GAD-AR and GAD-RA, (d) GO, GAD-AR-10 m and GAD-RA-10 m.

To detect the crystal structures of silver particles on hybrid materials, XRD patterns of RGO/silver were compared. As shown in Fig. 3c, the XRD results of as-synthesized GAD-AR and GAD-RA confirm the formation of face-centered cubic lattice crystal silver particles on graphene nanosheets, which are evidenced by the lattice face peaks (111), (200), (220), (311) and (222).[36] With regarding to those hybrid materials preserved for 10 months, some obvious differences can be observed between the XRD peaks of GAD-AR-10 m and GAD-RA-10 m. Observed from Fig. 3d, in the case of GAD-AR-10 m, the diffracting peaks corresponding to face-to-centre silver are similar with those peaks of freshly prepared GAD-AR. By contrast, for the GAD-RA-10 m, a new peaks at 32.1 ° ascribed to Ag_2O emerged, implying silver nanoparticles has been oxidized. In addition, it's noted that the peak intensity from the reflection of (200), (220), (311) and (222) crystal planes decreased, indicating oxidation reaction of silver particles are mainly occurred on the crystal plane with high surface energy.[36, 37]

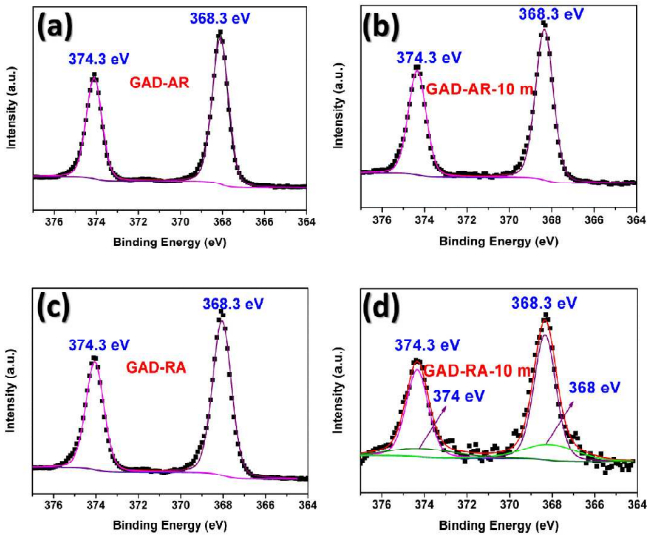

Fig. 4. Deconvoluted high resolution XPS spectra of Ag 3d: GAD-AR (a), GAD-AR-10 m (b), GAD-RA (c) and (d) GAD-RA-10 m.

With the aid of XPS, surface composition and chemical state of silver were further investigated. Because GO has been proved not a suitable substrate to suppress oxidation of silver particles, thus, the reduction of GO is important for the protection of silver particles.[38] Compared with C1s XPS spectrum of GO (shown in Fig. S1a), these peaks ascribed to RGO/silver hybrid materials (as shown in Fig. S2 and S3) with binding energy at 284.8 (C-C), 285.8 (C-O or C-N), 286.8 (C-O-C), 287.3 (C=O) and 288.6 eV (-COOH) decreased obviously after the decoration of silver particles, a clear indication that GO has been reduced. To confirm chemical state of silver particles on GAD after long-term storage, high resolution Ag 3d spectra of RGO/silver hybrid materials are presented in Fig. 4. As presented in Fig. 4a and 4c, two peaks appeared at 368.3 and 374.3 eV can be assigned to Ag $3d_{5/2}$ and Ag $3d_{3/2}$, respectively.[39] Therefore, the freshly synthesized silver particles in current study should be metallic Ag^0 as there is not any fitting component of silver oxidations. The chemical states of silver particles attached on the GAD-AR and GAD-RA exhibited totally different evolution after ten-month preservation. As shown in Fig. 4b and 4d, the two peaks at 368.3 and 374.4 eV from the case of GAD-AR-10 m are the same as those on GAD-AR and no extra fitting peak appears, suggesting the silver particles on the GAD-AR-10 m show excellent chemical stability. Nevertheless, two new peaks appeared at 368 and 374 eV can be observed from the high resolution XPS spectra of GAD-RA-10 m, implying a fraction of silver particles attached on the substrate have been partially oxidized.[40, 41] Therefore, by changing the sequence of "deoxygenation" and "deposition", it's clear that silver particles attached on the GAD-AR and GAD-RA show better chemical stability.

3.3 Proposed mechanism for chemical stability of silver particles

A mechanism is proposed to explain why the silver particles attached on the GAD-AR show better anti-oxidation performances. As reflected in models exhibited in Fig. 5a, RGO sheet is actually composed of oxidized and graphitic regions.[42-45] Considering the constrain effect from the oxygen-containing groups, silver particles were selectively distributed on the

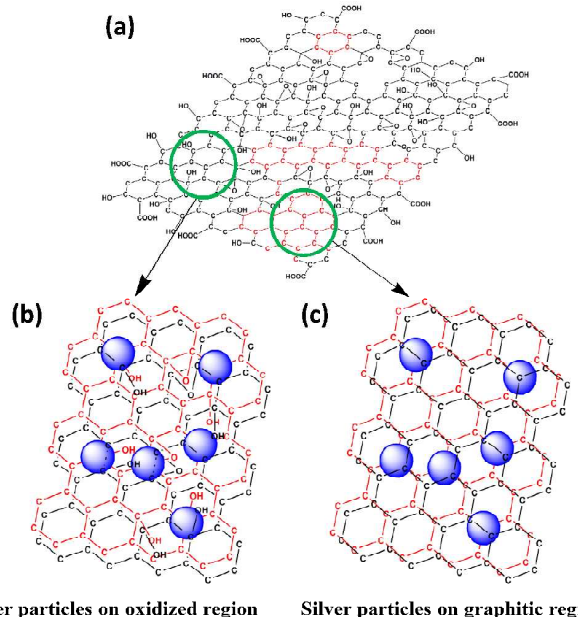

Fig. 5. (a) Model for the RGO: black zones stand for the oxidized regions while the red zones stand for graphitic regions, (b) Silver particles deposited on the oxidized region, (c) Silver particles deposited on graphitic region. Blue spheres present the silver particles. The electrons from silver particles that were located in oxidized regions are passivated by the electrophilic oxygen-containing groups and harder to be taken by the oxides. In comparison, the electrons of silver particles located at graphitic regions are surrounded by large amount of electrons and easy to be oxidized.

substrates via switching the sequence of "deoxygenation" and "deposition". For the case of GAD-AR, the silver particles were firstly deposited on GO before it was reduced, so the Coulombian force between positive silver anions and negative GO nanosheets made some reduced silver particles in-situ produced within the oxidized region that consists of abundant oxygen-containing groups (Fig. 5b). As the masking effect of attached particles and limited reducing ability of DMF, most silver particles on GAD-RA would be solidly stuck on the RGO substrates with residual oxygen-containing groups. As compared to GAD-AR, silver particles from GAD-RA were firstly deposited onto reduced GO, which preserved much less oxygen moieties than GO, thus most of silver particles were randomly distributed and most of them deposited on the graphitic regions where very few oxygen-containing groups exist, leading to weak interaction between particles and substrates (Fig. 5c). The different interaction between particles and substrate were confirmed by SEM and XPS results. From wide-scan XPS curves (as shown in Fig. S2b and S2d), for the freshly prepared hybrid materials, the silver loading of GAD-AR (20.7 wt%) is very close to that of GAD-RA (19.9 wt%). However, the mass loss of silver particles for GAD-AR and GAD-RA is apparently different after 10 months. As reflected in Fig. S3b and S3d, the XPS results indicate the residual loading of silver particles is 8.2 wt% for GAD-AR-10 m but only 2.4 wt% for GAD-RA-10 m. Obviously, in spite of weight losses are significant for both hybrid materials, more silver particles are preserved on GAD-AR-10 m than those on GAD-RA-10 m and that is consistent with situations reflected on Fig. 6, from which we can find far less particles reserved on GAD-RA-10 m (Fig. 6b) and these residual particles distribute on the

regions which are seriously wrinkled. By comparison, lots of silver particles can still be observed on GAD-AR-10 (Fig. 6a). On the other hand, oxygen containing groups would induce the formation of electron-rich regions due to its pull-electron effect.[46-48] When hybrid materials were attacked by oxides, silver nanoparticles located in electron-rich regions were supposed to be protected by electrons round them and relatively hard to be oxidized. On the contrast, silver particles deposited in electron-deficient regions would be easily oxidized since these silver particles were under less protection.

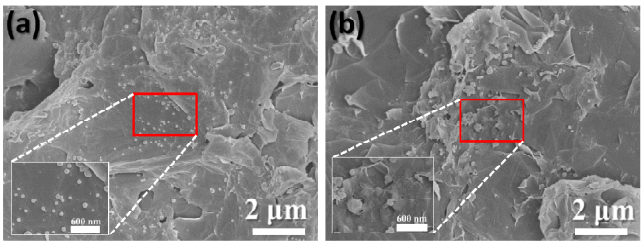

Fig. 6. The changes of the hybrids: SEM images of GAD-AR-10 m (a) and GAD-RA-10 m (Insets: enlarged images showing details of Ag particles deposited on RGO surface).

4. Conclusions

The RGO/silver hybrids were successfully prepared by switching the sequence of "deoxygenation" and "deposition". As DMF used here is not only solvent but the reductant, the sequence of "deposition" and "deoxygenation" can be controlled conveniently. Compared with GAD-RA-10 m, more silver particles are reserved on GAD-AR-10 m and SERS signals can still be observed after long-term storage. Silver particles decorated on GAD-AR exhibits much better chemical stability than those on GAD-RA. Based on selective distribution of silver particles and non-uniform dispersion of electrons on RGO nanosheets, a mechanism to explain the difference between GAD-AR and GAD-RA is proposed. The deep investigation of "deoxygenation" and "deposition" provides some illuminations for the preparation of chemically stable reduced graphene oxide/particle hybrid materials.

Acknowledgements

Yang is grateful for the financial support from the Materials Innovation for Marine and Offshore (MIMO) Program with the grant numbers SERC1123004032 and SERC 11230040288 under the Agency for Science, Technology and Research (A*Star) of Singapore

Notes and references

[a]School of Mechanical and Aerospace Engineering, Nanyang Technological University, Singapore 639798, Singapore. Email: MJLYang@ntu.edu.sg.

[b]School of Material Science and Engineering, Nanyang Technological University, Nanyang Avenue, 639798, Singapore. Email: asxhu@ntu.edu.sg.

†Electronic Supplementary Information (ESI) available: C1s and wide-scan XPS curves GO, GAD-AR, GAD-RA, GAD-AR-10 m and GAD-RA-10 m. **see doi: 10.1039/c000000x/**

1. S. Guo, S. Zhang, L. Wu and S. Sun, *Angewandte Chemie*, 2012, **51**, 11770-11773.
2. V. Singh, D. Joung, L. Zhai, S. Das, S. I. Khondaker and S. Seal, *Prog Mater Sci*, 2011, **56**, 1178-1271.
3. K. Gotoh, T. Kinumoto, E. Fujii, A. Yamamoto, H. Hashimoto, T. Ohkubo, A. Itadani, Y. Kuroda and H. Ishida, *Carbon*, 2011, **49**, 1118-1125.
4. H. Yin, C. Zhang, F. Liu and Y. Hou, *Advanced Functional Materials*, 2014, **24**, 2930-2937.
5. S.-H. Bae, K. Karthikeyan, Y.-S. Lee and I.-K. Oh, *Carbon*, 2013, **64**, 527-536.
6. H. Wang, Z. Xu, H. Yi, H. Wei, Z. Guo and X. Wang, *Nano Energy*, 2014, **7**, 86-96.
7. B. Chen, X. Liu, X. Zhao, Z. Wang, L. Wang, W. Jiang and J. Li, *Carbon*, 2014, **77**, 66-75.
8. Y. Sun, S. Yang, Y. Chen, C. Ding, W. Cheng and X. Wang, *Environmental science & technology*, 2015, **49**, 4255-4262.
9. Y. Sun, Q. Wang, C. Chen, X. Tan and X. Wang, *Environmental science & technology*, 2012, **46**, 6020-6027.
10. J. Chen, H. Bi, S. Sun, Y. Tang, W. Zhao, T. Lin, D. Wan, F. Huang, X. Zhou, X. Xie and M. Jiang, *Acs Applied Materials & Interfaces*, 2013, **5**, 1408-1413.
11. S. Dutta, C. Ray, S. Sarkar, M. Pradhan, Y. Negishi and T. Pal, *Acs Applied Materials & Interfaces*, 2013, **5**, 8724-8732.
12. J. Liang, L. Li, K. Tong, Z. Ren, W. Hu, X. Niu, Y. Chen and Q. Pei, *Acs Nano*, 2014, **8**, 1590-1600.
13. T. Tran Thanh, M. Castro, T. Y. Kim, K. S. Suh and J.-F. Feller, *Analytical and Bioanalytical Chemistry*, 2014, **406**, 3995-4004.
14. M. Losurdo, I. Bergmair, B. Dastmalchi, T.-H. Kim, M. M. Giangregroio, W. Jiao, G. V. Bianco, A. S. Brown, K. Hingerl and G. Bruno, *Advanced Functional Materials*, 2014, **24**, 1864-1878.
15. Y. Ahn, Y. Jeong and Y. Lee, *Acs Applied Materials & Interfaces*, 2012, **4**, 6410-6414.
16. J. Zhao, Z. Zhang, Z. Yu, Z. He, S. Yang and H. Jiang, *Applied Surface Science*, 2014, **289**, 89-96.
17. X. Y. Li, J. Li, X. M. Zhou, Y. Y. Ma, Z. P. Zheng, X. F. Duan and Y. Q. Qu, *Carbon*, 2014, **66**, 713-719.
18. Y. Liu, Y. Hu and J. Zhang, *Journal of Physical Chemistry C*, 2014, **118**, 8993-8998.
19. Y. Zhou, J. Yang, S. Ma, N. Zhao, X. Cheng and T. Zhong, *Monatshefte Fur Chemie*, 2014, **145**, 11-17.
20. W. Wei, K. Chen and G. Ge, *Advanced Materials*, 2013, **25**, 3863-3868.
21. J. H. Park, P. Ambwani, M. Manno, N. C. Lindquist, P. Nagpal, S.-H. Oh, C. Leighton and D. J. Norris, *Advanced Materials*, 2012, **24**, 3988-3992.
22. V. G. Kravets, R. Jalil, Y. J. Kim, D. Ansell, D. E. Aznakayeva, B. Thackray, L. Britnell, B. D. Belle, F. Withers, I. P. Radko, Z. Han, S. I. Bozhevolnyi, K. S. Novoselov, A. K. Geim and A. N. Grigorenko, *Scientific Reports*, 2014, **4**.
23. B. Zahed and H. Hosseini-Monfared, *Applied Surface Science*, 2015, **328**, 536-547.
24. X. Cai, M. Lin, S. Tan, W. Mai, Y. Zhang, Z. Liang, Z. Lin and X. Zhang, *Carbon*, 2012, **50**, 3407-3415.

25. X.-Z. Tang, Z. Cao, H.-B. Zhang, J. Liu and Z.-Z. Yu, *Chemical Communications*, 2011, **47**, 3084-3086.
26. X.-Z. Tang, X. Li, Z. Cao, J. Yang, H. Wang, X. Pu and Z.-Z. Yu, *Carbon*, 2013, **59**, 93-99.
27. G. Goncalves, P. A. A. P. Marques, C. M. Granadeiro, H. I. S. Nogueira, M. K. Singh and J. Grácio, *Chemistry of Materials*, 2009, **21**, 4796-4802.
28. H. Wang, H. S. Casalongue, Y. Liang and H. Dai, *Journal of the American Chemical Society*, 2010, **132**, 7472-7477.
29. J. I. Paredes, S. Villar-Rodil, A. Martinez-Alonso and J. M. D. Tascon, *Langmuir*, 2008, **24**, 10560-10564.
30. K. L. Ai, Y. L. Liu, L. H. Lu, X. L. Cheng and L. H. Huo, *J Mater Chem*, 2011, **21**, 3365-3370.
31. F. Y. Yuan, H. B. Zhang, X. F. Li, H. L. Ma, X. Z. Li and Z. Z. Yu, *Carbon*, 2014, **68**, 653-661.
32. W. S. Hummers and R. E. Offeman, *Journal of the American Chemical Society*, 1958, **80**, 1339-1339.
33. D. Li, M. B. Muller, S. Gilje, R. B. Kaner and G. G. Wallace, *Nat Nanotechnol*, 2008, **3**, 101-105.
34. S. T. He, J. N. Yao, P. Jiang, D. X. Shi, H. X. Zhang, S. S. Xie, S. J. Pang and H. J. Gao, *Langmuir*, 2001, **17**, 1571-1575.
35. Z. Zhang, F. G. Xu, W. S. Yang, M. Y. Guo, X. D. Wang, B. L. Zhanga and J. L. Tang, *Chemical Communications*, 2011, **47**, 6440-6442.
36. G. Wang, X. C. Ma, B. B. Huang, H. F. Cheng, Z. Y. Wang, J. Zhan, X. Y. Qin, X. Y. Zhang and Y. Dai, *J Mater Chem*, 2012, **22**, 21189-21194.
37. A. R. Tao, S. Habas and P. D. Yang, *Small*, 2008, **4**, 310-325.
38. L. Yuan, L. Jiang, J. Liu, Z. Xia, S. Wang and G. Sun, *Electrochimica Acta*, 2014, **135**, 168-174.
39. K. P. Xie, L. Sun, C. L. Wang, Y. K. Lai, M. Y. Wang, H. B. Chen and C. J. Lin, *Electrochimica Acta*, 2010, **55**, 7211-7218.
40. X. Y. Gao, S. Y. Wang, J. Li, Y. X. Zheng, R. J. Zhang, P. Zhou, Y. M. Yang and L. Y. Chen, *Thin Solid Films*, 2004, **455**, 438-442.
41. T. C. Kaspar, T. Droubay, S. A. Chambers and P. S. Bagus, *Journal of Physical Chemistry C*, 2010, **114**, 21562-21571.
42. A. Bagri, C. Mattevi, M. Acik, Y. J. Chabal, M. Chhowalla and V. B. Shenoy, *Nat Chem*, 2010, **2**, 581-587.
43. P. V. Kumar, N. M. Bardhan, S. Tongay, J. Q. Wu, A. M. Belcher and J. C. Grossman, *Nat Chem*, 2014, **6**, 151-158.
44. K. Erickson, R. Erni, Z. Lee, N. Alem, W. Gannett and A. Zettl, *Advanced Materials*, 2010, **22**, 4467-4472.
45. C. Gomez-Navarro, J. C. Meyer, R. S. Sundaram, A. Chuvilin, S. Kurasch, M. Burghard, K. Kern and U. Kaiser, *Nano Lett*, 2010, **10**, 1144-1148.
46. D. T. Phan and G. S. Chung, *J Phys Chem Solids*, 2013, **74**, 1509-1514.
47. K. A. Velizhanin, N. Dandu and D. Solenov, *Phys Rev B*, 2014, **89**.
48. H. Seo, S. Ahn, J. Kim, Y. A. Lee, K. H. Chung and K. J. Jeon, *Scientific Reports*, 2014, **4**.

